Assessing Impact of Heavily Aged Batteries on Hybrid Electric Vehicle Fuel Economy and Drivability

Assessing Impact of Heavily Aged Batteries on Hybrid Electric Vehicle Fuel Economy and Drivability

Pier Giuseppe Anselma[1,2], Phillip J. Kollmeyer[3], Stefano Feraco[1,2], Angelo Bonfitto[1,2], Giovanni Belingardi[1,2], Ali Emadi[3], Nicola Amati[1,2], Andrea Tonoli[1,2]
[1]Department of Mechanical and Aerospace Engineering (DIMEAS), Politecnico di Torino, Torino, Italy
[2]Center for Automotive Research and Sustainable Mobility (CARS), Politecnico di Torino, Torino, Italy
[3]McMaster Automotive Resource Center (MARC), McMaster University, Hamilton, ON, Canada

E-mail: pier.anselma@polito.it, stefano.feraco@polito.it

***Abstract*- This paper investigates the impact of battery ageing on the fuel economy and drivability capability of a power-split hybrid electric vehicle (HEV). The HEV is modelled first, an optimal energy management strategy based on dynamic programming is then implemented, and experimental characterization data for the battery cell is presented. The batteries are tested to a heavily aged state, with up to an 84% loss of capacity. Numerical simulations for the HEV performing the WLTP cycle and full power acceleration maneuvers are used to calculate the progressive worsening of fuel economy and rate of acceleration as the battery ages. The fuel economy and acceleration of the vehicle are found to be relatively unaffected until the battery loses more than 20% of original capacity. For the most aged case, with 84% loss of capacity, vehicle fuel economy increases by 25% and 0 to 100 km/h acceleration time reduces by 3.5 seconds compared to performance with a new battery.**

I. INTRODUCTION

Hybrid electric vehicles (HEVs) are a promising technology to reduce tailpipe emissions without depending on charging infrastructure like pure electric vehicles [1]. In HEVs, high-voltage batteries play a crucial role providing a second bidirectional energy source in the vehicle. Internal combustion engines (ICEs) in HEVs can operate more efficiently through their synergetic cooperation with the electric motor/generators (EMs) that are powered by batteries. Moreover, vehicle batteries enable storing electrical energy harvested in regenerative braking for future use as propelling energy [2]. It is therefore crucial that the battery operates effectively throughout the entire HEV lifetime, even as the battery ages significantly [3].

As batteries age their properties change; internal electrical resistance increases, capacity decreases, and the open-circuit voltage characteristics may change, leading to reduced capability [4][5]. Ageing of high-voltage batteries for electrified vehicles is a growing research topic as electrified vehicles become more prevalent and those in the field reach an advanced stage of life.

Research studies have considered how battery ageing impacts a few types of vehicles. Herb et al. in 2013 modeled the performance variation for a fuel cell electric vehicle by assuming the battery power capability linearly decreases over time [6]. In 2015, Saxena et al. studied how battery capacity fade and reduced power capability impacts the ability of pure electric vehicles to satisfy daily travel needs [7]. The study suggested that batteries could meet driver needs well after the battery has lost 20-30% of capacity, which is the threshold often considered to be end-of-life. The potential for batteries to perform functionally even when highly aged inspired this work, which investigates how well an HEV performs after the battery loses more than 80% of initial capacity. Such analysis allows providing an estimate to the HEV user of how much fuel consumption increases and acceleration capability decreases as the high-voltage battery progressively ages. The HEV user could in turn decide whether to replace the battery pack at the conventional end-of-life limit of 80% residual capacity or to maintain the same battery pack until the loss of capacity and power capability results in unacceptable performance. Residual capacity, the ratio of current capacity to capacity at beginning of life, is defined as state of health (SOH) for this research. Even though high-voltage batteries can be reused in a second-life operation [8], replacing an HEV battery pack is a costly operation for the user and involves additional CO_2 emissions to produce a new battery pack, thus providing further motivation for the presented work.

The paper is organized as follows: the HEV model and the adopted simulation approach are presented first. Experimental results for three cells are then presented, including residual capacity and power capability at various ageing conditions. Results are presented for HEV simulations conducted at different levels of battery SOH to assess fuel economy potential and acceleration capability, and conclusions are given.

II. HEV MODEL AND CONTROL STRATEGY

A. Representative HEV

The HEV powertrain architecture investigated in this study is representative of the third generation Toyota Prius® hybrid. A spark-ignition Atkinson ICE and two EMs are used in the HEV. The ICE, EM1 and final drive input shaft are respectively linked to the carrier, sun gear, and ring gear of a

TABLE I
ASSUMED HEV PARAMETERS

Component	Parameter	Value
Vehicle	Mass	1531 kg
ICE	Capacity	1.8 L
	Power max	72 kW @ 5,000 rpm
	Torque max	142 Nm @ 4,000 rpm
EM1	Power max	42 kW
EM2	Power max	65 kW
Transmission	PG ratio (Ring / Sun)	2.6
	Gear ratio (EM2)	1.26
	Final drive ratio	3.27
	Efficiency (EV mode)	0.95
	Efficiency (HEV mode)	0.85
Auxiliaries	Electrical subsystem power	500 W
Battery	Pack capacity	1.82 kWh
	Pack configuration	120S – 2P
	Cell type	A123 ANR26650M1-B

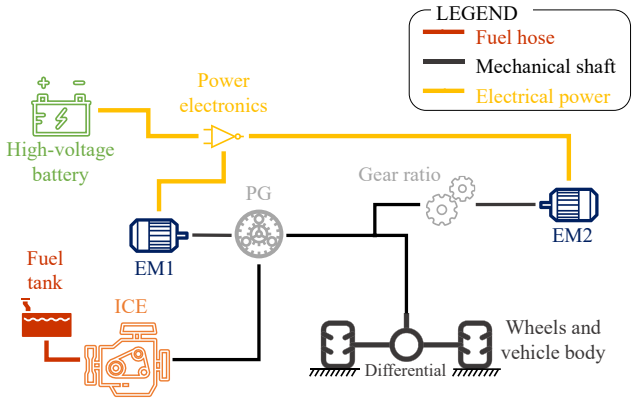

Fig. 1 Toyota Prius hybrid electric powertrain scheme.

planetary gear (PG) set, a mechanical device that allows decoupling the speed of the ICE and EM1 from the speed of the vehicle. This HEV powertrain is a well-known layout from the state-of-the-art, and open-source data regarding it is available [9]. The HEV parameters used in this analysis are reported in Table 1, while the hybrid powertrain configuration is illustrated in Fig. 1. The battery pack has been assumed in this case to consist of quantity 240 A123 ANR26650M1-B cells in a 120 series, 2 parallel (120S2P) configuration, since these cells from A123 were tested experimentally as described in Section III. The investigated 1.8 kWh pack has somewhat more capacity than the 3rd Gen Prius's 1.3kWh NiMH battery pack.

B. *Modeling approach*

The HEV powertrain is modeled using a backward quasi-static approach to derive the requested power values and the speed of components directly from the driving mission requirements (i.e. vehicle speed and acceleration over time). Fuel consumption as well as EM loss is evaluated by means of empirical lookup tables with speed and torque as independent variables [10]. For the battery, an equivalent circuit model is adopted with open-circuit voltage, internal resistance, charge power capability, discharge power capability and residual capacity values depending on the instantaneous values of both state of charge (SOC) and SOH [11][12].

C. *Fuel economy assessment*

To estimate the fuel economy of the HEV, an appropriate energy management strategy needs to be implemented. In this case, the HEV energy management strategy selects at each time instant either pure electric or hybrid operation. If pure electric operation is selected, only EM2 is activated to either propel the vehicle or to recover electrical energy during regenerative braking. On the other hand, if hybrid mode is enabled, the ICE is in operation and the controller selects the values of ICE speed and ICE torque. In a backward quasi-static approach, knowing speed and torque of the ICE allows automatically determining speed and torque values for the EMs based on the gear ratios. Once speed and torque of the components are known, the instantaneous fuel consumption rate and battery SOC variation can be easily determined. The reader can find details regarding the HEV modeling approach and the related equations in [13].

Dynamic programming (DP) is used here to create a globally optimal HEV control approach. As an off-line method, DP requires the knowledge of the vehicle speed profile for the entire drive cycle before performing the simulation [14]. While DP cannot practically be applied in a vehicle due to its off-line nature and computational cost, DP does provide an upper bound for how well a control policy could perform for this HEV architecture [15]. In this case, DP controls the speed and torque of the ICE and EMs to minimize fuel consumption solely over a predefined drive cycle while sustaining battery charge and limiting the overall number of ICE activations. The cost function J that is minimized with DP over a given drive cycle and the related HEV operational constraints are reported in (1):

$$J = \int_{t_0}^{t_{end}} \left[\dot{m}_{fuel}(t) + \mu_{crank} \cdot start_{ICE}(t)\right] dt$$

subject to:

Mechanical constraints:

$$\begin{gathered} ICE_{on/off}(t)=[0,1] \\ 0 \le \omega_{ICE}(t) \le \omega_{ICE_{MAX}} \\ \omega_{EM1_{min}} \le \omega_{EM1}(t) \le \omega_{EM1_{MAX}} \\ 0 \le \omega_{EM2}(t) \le \omega_{EM2_{MAX}} \\ 0 \le T_{ICE}(t) \le T_{ICE_{MAX}}[\omega_{ICE}(t)] \\ T_{EM1_{min}}[\omega_{EM1}(t)] \le T_{EM1}(t) \le T_{EM1_{MAX}}[\omega_{EM1}(t)] \\ T_{EM2_{min}}[\omega_{EM2}(t)] \le T_{EM2}(t) \le T_{EM2_{MAX}}[\omega_{EM2}(t)] \end{gathered} \quad (1)$$

Battery constraints:

$$\begin{gathered} SOC(t_0) \le SOC(t_{end}) \le SOC(t_0) + \delta \\ P_{batt-min}(SOC, SOH) \le P_{batt}(t) \\ \le P_{batt-MAX}(SOC, SOH) \\ SOC_{min} \le SOC(t) \le SOC_{MAX} \\ c(t) \le c_{MAX} \end{gathered}$$

where $\dot{m}_{fuel}$ and μ_{crank} are the fuel rate consumed by the ICE at each time instant (as computed following the HEV model described) and a constant penalization term for cranking the ICE, respectively. The parameter $start_{ICE}$ represents a binary flag detecting ICE cranking events. When solving the optimal HEV control problem, imposed mechanical constraints involve limiting torque (denoted as T) and speed (denoted as ω) of the power components within the corresponding allowed operating regions. $ICE_{on/off}$ is a binary variable for the ICE state, and values of 0 and 1 relate to the ICE being off and on, respectively. The battery SOC is set to have similar values at the beginning (i.e. $t = t_0$) and end (i.e. $t = t_{end}$) of the drive cycle assuming an appropriate tolerance δ. Finally, both battery SOC, battery C-rate and battery power are constrained within the corresponding allowed operating regions. Battery charge and discharge power limits are calculated based on the SOC and SOH dependent resistance. The charge power is particularly important because it limits how much energy can be captured from regenerative braking. Any energy which cannot be captured is dissipated by friction braking. Moreover, only friction braking is assumed to operate here below vehicle speed values of 10 km/h, given the limited amount of kinetic energy available to capture at low vehicle speeds [16].

When solving the control problem backwardly from the last time instant of the drive cycle, DP considers the state variables which are the parameters whose evolution throughout the drive cycle depends on the preceding time steps [17]. The states X for the HEV powertrain layout are battery SOC and the ICE on/off state as reported in (2), The Control variables U are also listed in (2), and include ICE speed and torque as discussed at the beginning of this sub-section:

$$X = \begin{Bmatrix} SOC(t) \\ ICE_{on/off}(t) \end{Bmatrix}; \quad U = \begin{Bmatrix} \omega_{ICE}(t) \\ T_{ICE}(t) \end{Bmatrix} \qquad (2)$$

where battery SOC is managed to guarantee charge-sustenance and the ICE state (i.e. on/off) is considered to limit the frequency of cranking events to a reasonable value.

When solving optimal HEV control problems, there are typically some operating points that are very efficient, which may lead to binary controlled variables (e.g. ICE de/activation) toggling a lot to maximize operation at these high efficiency points [18]. Therefore, it is necessary to constrain the ICE cranking frequency to create a control policy which is feasible in the real-world. The DP implemented in MATLAB© software in this work uses the open-source function provided by Sundstrom and Guzzella [19].

D. Acceleration capability assessment

Other than fuel economy potential, the drivability of the HEV is evaluated as a function of battery SOH. To this end, three full power acceleration maneuvers are considered: 0-30 km/h, 30-60 km/h and 60-100 km/h. The time required for the HEV to complete each acceleration maneuver is determined and used as evaluation metric for the drivability of the HEV as function of battery SOH. The same HEV numerical model used for the fuel economy assessment and implemented in MATLAB© software is considered. However, instead of evaluating the HEV powertrain consumption in terms of fuel and battery energy, the maximum amount of tractive power deliverable by the power components is used to simulate the HEV acceleration capability [20]. The time to accelerate to a given speed increases with ageing due to significantly reduced battery power capability.

III. CELL EXPERIMENTAL CHARACTERIZATION AT VARIOUS SOH VALUES

In a previous work, the authors performed an experimental campaign assessing the ageing behavior of three A123 ANR26650M1-B cells subjected to different current profiles associated with an HEV performing the worldwide harmonized light-vehicle test procedure (WLTP) cycle. The current profiles were designed using a numerical ageing model to age the battery after approximately 100 thousand, 200 thousand, and 300 thousand km of driving. The three battery cells are referred to in this work as “Batt1”, “Batt2” and “Batt3”, respectively.

The experimental setup and the trend of the residual capacity over time for the tested cells are shown in Fig. 2 and Fig. 3, respectively, while more details regarding the experimental campaign can be found in [21]. Specifically, the cells were placed in an Envirotronics SH16C thermal chamber and temperature was regulated to 25°C. A ±75A, 0–5 V rated channel of an MCT 75–0/5-8ME Digatron Power Electronics battery cycler was used to test each cell. Cell voltage was measured at the battery terminals via the battery cycler and a temperature sensor was fixed to the front center face of the cell.

Fig. 2 Experimental setup for tested cells.

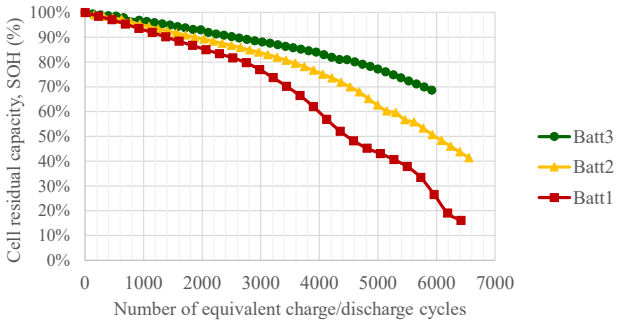

Fig. 3 Trend of residual capacity over time for tested cells.

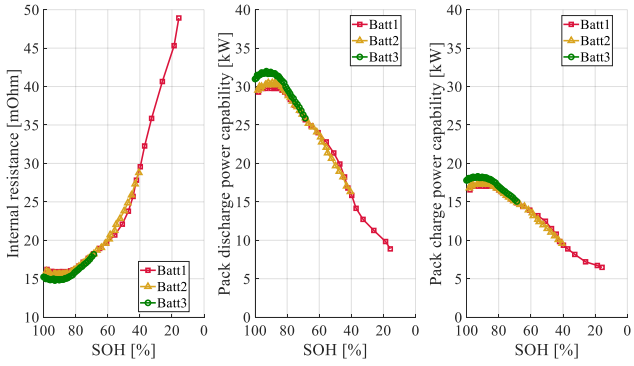

(a) Internal resistance (b) Discharge power capability (c) Charge power capability

Fig. 4 Experimentally determined cell internal resistance and calculated pack power capability of the tested cells at 50% SOC and as function of SOH.

The voltage and current measurement and control accuracy of the battery cycler is ±0.1% of full scale and the accuracy of the temperature sensor is ±0.5°C. The cycler can regulate voltage from 0 V to 5 V, current from -75A to 75A, and power from -375W to 375 W. The battery cycler utilizes an automated software, named "Battery Manager", which is provided by Digatron. It runs on a desktop computer and can be used to create test programs and to save the results in a database. Each program consists of thousands of steps which can be a pause, constant voltage, constant current, or constant power step, or a power or current profile, as used for the WLTP cycles in this specific case.

Fig. 4(a) shows that internal cell resistance at 50% SOC is relatively constant until 80% SOH, and then steadily increases and doubles by around 40% SOH. Resistance was calculated from a hybrid pulse power characterization (HPPC) test which was repeated periodically throughout the ageing tests. Increased resistance results in reduced pack power capability, as is illustrated in Fig. 4(b) and (c) for 50% SOC, an upper battery cell voltage limit of 3.6V, a lower limit of 2.5V, and 240 cells. These plots, which were not published in the prior work in [21], are used as lookup tables in the HEV model illustrated in Section 2. Specifically, the considered battery modeling approach updates the open-circuit voltage and resistance values with respect to the SOC characteristic for each value of the SOH. Then, the charge and discharge power capability is computed at every time step of the simulation, while respecting the voltage limits. An in-depth description of the battery ageing modeling approach which is used can be found in [21], assuming a lumped cell temperature equal to 25 °C.

The analysis uses data for each cell from beginning of life (100% SOH) to the end of the test, 16%, 40% and 69% SOH for the "Batt1", "Batt2" and "Batt3" test cases, respectively.

IV. Simulation Results At Varying Battery Ageing Conditions

This section illustrates the simulation results obtained for the power-split HEV powertrain at varying battery ageing conditions in terms of fuel economy potential and drivability. High-voltage battery SOH values from 95% to 16% in 5% steps are considered. HEV fuel economy capability as predicted by DP simulations of the WLTP cycle are first assessed. Then HEV performance for the WLTP cycle at beginning, middle, and end of life, i.e. 95%, 55% and 16% SOH, is compared. Drivability performance for full power acceleration maneuvers is then presented.

A. Impact of ageing on fuel consumption

HEV fuel consumption obtained by DP for the WLTP cycle is presented as a function of SOH in Fig. 5. Fuel consumption is calculated for each of the three aged batteries (i.e. "Batt1", "Batt2" and "Batt3"), demonstrating that fuel economy is mostly dependent on SOH and not on how the battery was aged. For the new battery, fuel consumption is estimated by DP to be approximately 3.91 l/100km for the WLTP drive cycle, which is about 17% less than the 4.7 l/100km which the model year 2010 Toyota Prius® Hybrid is rated for [22]. Considering that the vehicle's rated fuel economy is calculated from weighted UDDS and HWFET cycles scaled by a correction factor, the model fuel economy matches the rated fuel economy rather well. Several aspects of the modeling may also contribute to the difference, including (1) the simplified HEV modelling approach, which neglects transient phenomena and thermal aspects; (2) the lookup tables used for modeling power components; (3) the considered cell type (i.e. A123 ANR26650M1-B), which is different than the cells used in the Prius®; and (4) the HEV energy management strategy, since DP is different than a real time control strategy.

In Fig.5, fuel consumption is shown to be relatively flat during the first 20% of ageing, with fuel consumption only

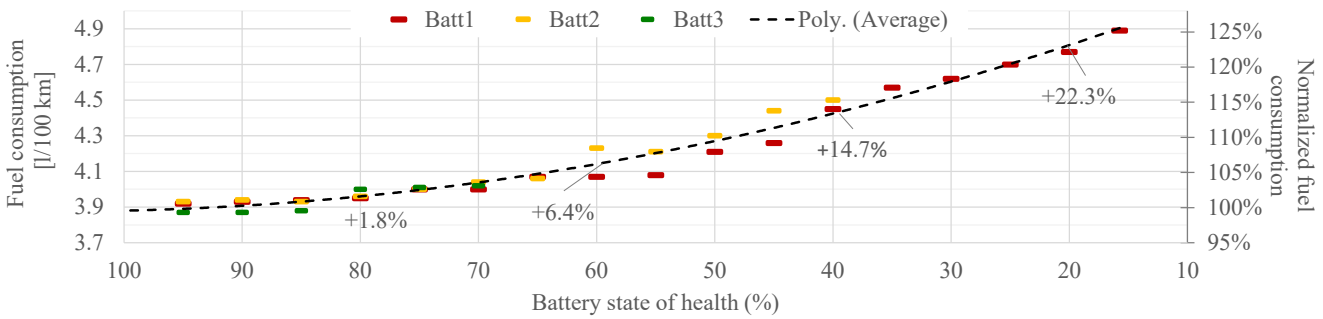

Fig. 5 HEV fuel economy capability predicted by DP in the WLTP over retained battery SOH values for the three test cases and related average.

increasing by 1.8% at 80% SOH. Beyond 80% SOH fuel consumption starts to increase significantly, reaching a 10% increase at 50% SOH, and a 25.2% increase at 16% SOH. These results suggest that beyond 80% SOH, and especially beyond 50% SOH, there will be noticeable fuel economy benefits when replacing the pack.

B. Impact of ageing on battery use during WLTP cycle

To demonstrate how the powertrain's use of the battery varies with ageing, the powertrain performance is simulated using DP for 95%, 55%, and 16% SOH data for *Batt1*. Fig. 6 illustrates battery pack power and net charge in amp-hours over time for the three ageing cases, while Table II reports corresponding loss and performance statistics for the overall drive cycle. In particular, electric motor losses are obtained by interpolating in the electrical loss tables as function of speeds and torques of the corresponding power components in the overall drive cycle. Friction brake loss are calculated by integrating the friction brake power contribution throughout the drive cycle. Battery loss derives from the integration of the instantaneous internal resistance multiplied by the squared instantaneous current. Finally, ICE mechanical energy corresponds to the integration of the engine rotational speed multiplied by the engine torque.

As the cell ages, power capability and capacity are reduced, resulting in a substantial reduction of charge and discharge current and consequently net charge used from the battery as is seen in Fig. 6. This reduced use of the battery has two primary impacts on vehicle fuel economy. First, the battery is capable of capturing much less regenerative braking energy, resulting in around eight times more friction brake loss when SOH has reduced to 16%, as shown in Table II. Second, the system is not able to shut the engine off as often and operate only at the most efficient points, causing engine efficiency to reduce from 38% to 34%, as also shown in Table II.

Table II also shows that EM1, which is linked directly with the ICE via the planetary gearbox, has loss increase with battery ageing due to increased use of the ICE. EM2 loss decreases by a similar amount though, due to less time spent in electric mode. Even though battery resistance increases with age, battery loss ends up decreasing as the battery ages because loss is a quadratic function and power capability is linear, meaning loss falls faster than power capability.

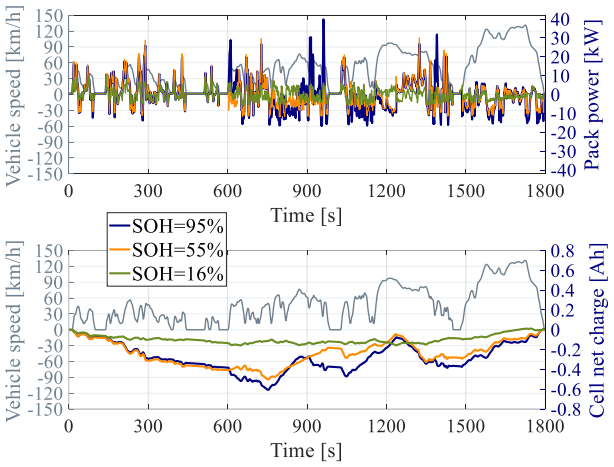

Fig. 6 Battery pack power and SOC as predicted by DP in WLTP for battery SOH values corresponding to 95%, 55% and 16% of "Batt1".

TABLE II
STATISTICS OF THE HEV OPERATION CONTROLLED BY DP IN WLTP FOR BATTERY SOH VALUES OF 95%, 55% AND 16% OF "BATT1"

	SOH=95%	**SOH=55%**	**SOH=16%**
EM1 loss [kJ]	238	269	422
EM2 loss [kJ]	1063	999	750
Friction brake loss [kJ]	215	560	1645
Battery loss [kJ]	607	581	273
ICE off time [%]	70.9	63.6	27.9
Fuel consumption [g]	670.4	705.5	845.4
ICE mechanical energy [kJ]	10937	11333	12399
Average ICE efficiency [%]	38	38	34

C. Drivability

To characterize the drivability of the HEV, three full power accelerations were simulated: 0-30 km/h, 30-60 km/h and 60-100 km/h. The time required to complete each of the three maneuvers is plotted in Fig. 7 for different levels of battery ageing, assuming battery characteristics at each SOH are an average of the three test cases. With a new battery the vehicle can accelerate from 0-100 km/h in 9.8 seconds, and this increases by 5.1%, 11.2%, 22.4% and 35.7% at SOH values of 80%, 60%, 40% and 16%, respectively. The acceleration rate is relatively stable until 80% SOH and increases substantially with further ageing. The 60-100 km/h acceleration time is most

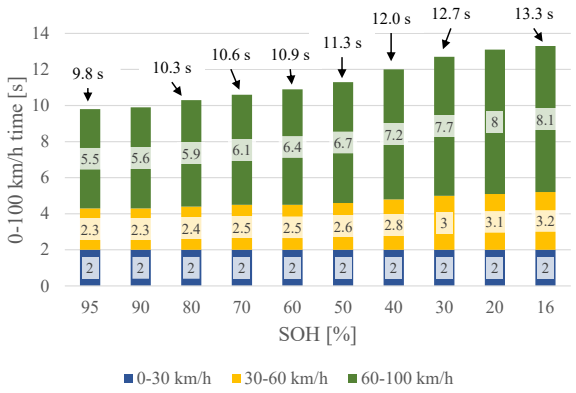

Fig. 7 HEV acceleration performance in 0-30km/h, 30-60 km/h and 60-100 km/h full power acceleration maneuvers over retained battery SOH values.

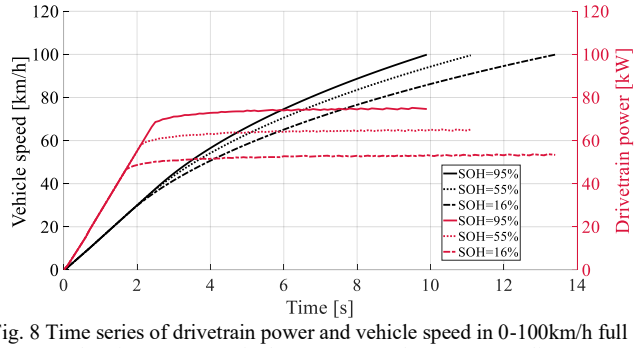

Fig. 8 Time series of drivetrain power and vehicle speed in 0-100km/h full power acceleration maneuver for battery SOH values corresponding to 95%, 55% and 16% of "Batt1".

affected because the drivetrain is operating in the peak power region here, rather than in the peak torque region as at lower speeds. Peak battery pack power is reduced considerably with ageing, as shown in Fig. 4. This in turn affects the maximum tractive power deliverable by the drivetrain, as can be seen in Fig. 8 which shows drivetrain power and vehicle speed for 0-100km/h full power accelerations for different states of ageing of *Batt1*. The drivetrain peak tractive power, depending on ICE, EM1, EM2, battery, and transmission power, reduces from 74kW for new battery conditions to 64kW for SOH=55% down to 53kW when SOH=16%. These results demonstrate that power capability reduces steadily with battery ageing.

V. CONCLUSIONS

Hybrid electric vehicle batteries continue to function well beyond the 80% SOH value which is often considered end of life. As battery capacity degrades power capability decreases as well, preventing the vehicle from accelerating as quickly and recapturing as much regenerative braking energy as when the vehicle was new. The loss of battery capacity and power capability also results in the ICE operating more frequently and at less efficient operating points. For the HEV investigated in this study using experimentally derived battery characteristics, these factors combine to cause a 6% increase in fuel consumption at 60% SOH and a much greater 25% increase at 16% SOH. 0 to 100 km/h acceleration time also increases significantly as the battery ages, going from 9.8 s when new to 13.3 s at 16% SOH.

While this study investigates performance degradation of cylindrical lithium iron phosphate ($LiFePO_4$) cells, the same approach could be applied for battery packs using nickel manganese cobalt oxide (NMC) or nickel cobalt aluminum oxide (NCA) Li-ion cells or nickel metal hydride (NiMH) cells, which are commonly used in electrified vehicles. An extensive experimental validation would be needed to conclusively determine the proposed method can be applied generally for any battery pack.

In general, the obtained results can be used to determine when an HEV user is likely to benefit from replacing the battery pack due to excessive ageing. Furthermore, the HEV simulations performed as the battery ages may be useful for developing more accurate battery state estimation algorithms, robust battery management systems and HEV energy management strategies capable of adapting to the SOH of the high-voltage battery pack.

REFERENCES

[1] B. Bilgin et al., "Making the Case for Electrified Transportation," in *IEEE Transactions on Transportation Electrification*, vol. 1, no. 1, pp. 4-17, 2015.

[2] A. Emadi, "Transportation 2.0: Electrified-enabling cleaner, greener, and more affordable domestic electricity to replace petroleum," IEEE Power Energy Mag., vol. 9, no. 4, pp. 18–29, Jul./Aug. 2011.

[3] A. Bonfitto, "A Method for the Combined Estimation of Battery State of Charge and State of Health Based on Artificial Neural Networks," *Energies*, vol. 13, no. 10, pp. 2548-2560, 2020.

[4] R. Xiong, Y. Pan, W. Shen, H. Li, F. Sun, "Lithium-ion battery aging mechanisms and diagnosis method for automotive applications: Recent advances and perspectives," *Renewable and Sustainable Energy Reviews*, vol 131, no. 110480, pp. 1-14, 2020.

[5] "Battery Test Manual for Plug-In Hybrid Electric Vehicles," U.S. Department of Energy, Idaho National Laboratory, Idaho Falls, Idaho 83415, March 2008.

[6] F. Herb, P. R. Akula, K. Trivedi, L. Jandhyala, A. Narayana, M. Wöhr, "Theoretical analysis of energy management strategies for Fuel Cell Electric Vehicle with respect to fuel cell and battery aging," *2013 World Electric Vehicle Symposium and Exhibition (EVS27)*, Barcelona, 2013, pp. 1-9

[7] S. Saxena, C. Le Floch, J. MacDonald, S. Moura, "Quantifying EV battery end-of-life through analysis of travel needs with vehicle powertrain models," *J. Power Sources*, vol. 282, pp.265-276, 2015.

[8] G Filomeno, S. Feraco, "Economic, Technical and Environmental Aspects of Recycling Lithium Batteries: A Literature Review," *Global Journal of Researches in Engineering: B Automotive Engineering*, vol 20, no. 1, pp. 1-8, 2020.

[9] S. Lee, B. Lee, J. McDonald, L. Sanchez et al., "Modeling and Validation of Power-Split and P2 Parallel Hybrid Electric Vehicles," *SAE Technical Paper* 2013-01-1470, 2013.

[10] G. Rizzoni, L. Guzzella, B. M. Baumann, "Unified modeling of hybrid electric vehicle drivetrains," *IEEE/ASME Transactions on Mechatronics*, vol. 4, no. 3, pp. 246-257, Sept. 1999.

[11] A. Bonfitto, E. Ezemobi, N. Amati, S. Feraco, A. Tonoli, S. Hegde, "State of Health Estimation of Lithium Batteries for Automotive Applications with Artificial Neural Networks," *2019 AEIT International Conference of Electrical and Electronic Technologies for Automotive (AEIT AUTOMOTIVE)*, Torino, Italy, 2019, pp. 1-5.

[12] A. Bonfitto, S. Feraco, A. Tonoli, N. Amati, F. Monti, "Estimation Accuracy and Computational Cost Analysis of Artificial Neural Networks for State of Charge Estimation in Lithium Batteries," *Batteries*, vol. 5, no. 2, pp. 47-63, 2019.

[13] P. G. Anselma, P. Kollmeyer, G. Belingardi, A. Emadi, "Multi-Objective Hybrid Electric Vehicle Control for Maximizing Fuel Economy and Battery Lifetime," *2020 IEEE Transportation Electrification Conference & Expo (ITEC)*, Chicago, IL, USA, 2020, pp. 1-6.

[14] L. Bruck, A. Lempert, S. Amirfarhangi Bonab, J. Lempert et al., "A Dynamic Programming Algorithm for HEV Powertrains Using Battery Power as State Variable," *SAE Technical Paper* 2020-01-0271, 2020.

[15] P.G. Anselma, A. Biswas, G. Belingardi, A. Emadi, "Rapid assessment of the fuel economy capability of parallel and series-parallel hybrid electric vehicles," *Applied Energy*, vol. 275, no. 115319, 2020.

[16] P.G. Anselma, G. Belingardi, "Multi-objective optimal computer-aided engineering of hydraulic brake systems for electrified road vehicles," *Vehicle System Dynamics*, in press, 2021.

[17] P. Elbert, S. Ebbesen, L. Guzzella, "Implementation of Dynamic Programming for n-Dimensional Optimal Control Problems With Final State Constraints," in *IEEE Transactions on Control Systems Technology*, vol. 21, no. 3, pp. 924-931, May 2013.

[18] S. Delprat, T. Hofman, S. Paganelli, "Hybrid Vehicle Energy Management: Singular Optimal Control," IEEE Transactions on Vehicular Technology, vol. 66, no. 11, pp. 9654-9666, 2017.

[19] O. Sundstrom, L. Guzzella, "A generic dynamic programming Matlab function," 2009 IEEE Control Applications, (CCA) & Intelligent Control, (ISIC), St. Petersburg, 2009, pp. 1625-1630.

[20] P. G. Anselma, C. Boursier Niutta, L. Mainini, G. Belingardi, "Multidisciplinary design optimization for hybrid electric vehicles: component sizing and multi-fidelity frontal crashworthiness," *Structural and Multidisciplinary Optimization*, vol. 62, pp. 2149-2166, 2020.

[21] P. G. Anselma, P. Kollmeyer, J. Lempert, Z, Zhao, G. Belingardi, A. Emadi, "Battery State-of-Health Sensitive Energy Management of Hybrid Electric Vehicles: Lifetime Prediction and Ageing Experimental Validation," *Applied Energy*, vol. 285, no. 116440, 2021.

[22] US EPA, "Fuel economy of the 2010 Toyota Prius," [online], available: https://www.fueleconomy.gov/feg/noframes/26425.shtml (accessed 2 Apr. 2021).